Exploring label dynamics of velocity-selective arterial spin labeling in the kidney

Bones, I.K.; Franklin, S.L.; Harteveld, A.A.; Osch, M.J.P. van; Schmid, S.; Hendrikse, J.; ... ; Bos, C.

Received: 16 October 2020 | Revised: 7 December 2020 | Accepted: 24 December 2020

DOI: 10.1002/mrm.28683

FULL PAPER

Magnetic Resonance in Medicine

Exploring label dynamics of velocity-selective arterial spin labeling in the kidney

Isabell K. Bones[1] | **Suzanne L. Franklin**[1,2] | **Anita A. Harteveld**[1,3] | **Matthias J. P. van Osch**[2] | **Sophie Schmid**[2] | **Jeroen Hendrikse**[4] | **Chrit Moonen**[1] | **Marijn van Stralen**[1] | **Clemens Bos**[1]

[1]Center for Image Sciences, University Medical Center Utrecht, Utrecht, the Netherlands

[2]C.J. Gorter Center for High Field MRI, Department of Radiology, Leiden University Medical Center, Leiden, the Netherlands

[3]Department of Radiology and Nuclear Medicine, Erasmus MC University Medical Center Rotterdam, Rotterdam, the Netherlands

[4]Department of Radiology, University Medical Center Utrecht, Utrecht, the Netherlands

Correspondence
Isabell K. Bones, Center for Image Sciences, University Medical Center Utrecht, Heidelberglaan 100, 3584 CX Utrecht, the Netherlands.
Email: i.k.bones@umcutrecht.nl

Funding information
Applied and Engineering Sciences Research Program (Grant/Award No. 14951), which is partly financed by the Netherlands Organization for Scientific Research

Purpose: Velocity-selective arterial spin labeling (VSASL) has been proposed for renal perfusion imaging to mitigate planning challenges and effects of arterial transit time (ATT) uncertainties. In VSASL, label generation may shift in the vascular tree as a function of cutoff velocity. Here, we investigate label dynamics and especially the ATT of renal VSASL and compared it with a spatially selective pulsed arterial spin labeling technique, flow alternating inversion recovery (FAIR).

Methods: Arterial spin labeling data were acquired in 7 subjects, using free-breathing dual VSASL and FAIR with five postlabeling delays: 400, 800, 1200, 2000, and 2600 ms. The VSASL measurements were acquired with cutoff velocities of 5, 10, and 15 cm/s, with anterior–posterior velocity-encoding direction. Cortical perfusion-weighted signal, temporal SNR, quantified renal blood flow, and arterial transit time were reported.

Results: In contrast to FAIR, renal VSASL already showed fairly high signal at the earliest postlabeling delays, for all cutoff velocities. The highest VSASL signal and temporal SNR was obtained with a cutoff velocity of 10 cm/s at postlabeling delay = 800 ms, which was earlier than for FAIR at 1200 ms. Fitted ATT on VSASL was ≤ 0 ms, indicating ATT insensitivity, which was shorter than for FAIR (189 ± 79 ms, $P < .05$). Finally, the average cortical renal blood flow measured with cutoff velocities of 5 cm/s (398 ± 84 mL/min/100 g) and 10 cm/s (472 ± 160 mL/min/100 g) were similar to renal blood flow measured with FAIR (441 ± 84 mL/min/100 g) ($P > .05$) with good correlations on subject level.

Conclusion: Velocity-selective arterial spin labeling in the kidney reduces ATT sensitivity compared with the recommended pulsed arterial spin labeling method, as well as if cutoff velocity is increased to reduce spurious labeling due to motion. Thus, VSASL has potential as a method for time-efficient, single-time-point, free-breathing renal perfusion measurements, despite lower tSNR than FAIR.

KEYWORDS
arterial spin labeling, Buxton curve, FAIR, multi-PLD ASL, renal perfusion, velocity-selective labeling

1 | INTRODUCTION

Renal perfusion is a potentially valuable indicator of renal function,[1] which can be imaged noninvasively using arterial spin labeling (ASL) MRI.[2,3] Arterial spin labeling magnetically labels protons of blood, thereby creating an endogenous tracer, and does not require administration of a contrast agent. This makes it highly attractive for patients with renal impairment for whom use of contrast agents is not desirable and potentially dangerous. Quantitative values for renal blood flow (RBF) are useful for diagnostic purposes, monitoring perfusion changes over time in clinical practice, as well as clinical research. To quantify perfusion, ASL measurements need to be fitted to a model describing the blood label kinetics and relaxation processes over time.[4] A number of parameters need to be provided to the model that either have to be assumed based on literature values or determined by additional measurements. Arguably the most important parameter is the arterial transit time (ATT), which is the time it takes the arterial blood to travel from the labeling site to the capillaries in the tissue being imaged. The ATT can vary due to physiology status associated with age and gender, or pathology (eg, renal stenosis),[5-7] and without (or incorrectly) estimating the ATT, RBF accuracy will decrease and possibly lead to compromised interpretation. Commonly applied ASL techniques, which use spatially selective labeling of blood, are intrinsically ATT-sensitive, as the label is created at a location upstream of the imaging volume, which subsequently flows to the target tissue before ASL image readout.[8] One of the oldest spatially selective ASL methods, flow alternating inversion recovery (FAIR) ASL,[9] was recently recommended for renal perfusion measurement.[3]

Flow-sensitized ASL is a more recent approach that can potentially mitigate ATT effects and could allow single-time-point ASL with minimal confounding effects of ATT.[10-14] Several flow-based ASL techniques have been developed until now, including velocity-selective ASL (VSASL).[10,11,15] Here, blood is saturated when its flow velocity exceeds a chosen cutoff velocity (V_C). By choosing V_C low enough, label is generated even in small vessels and therefore also within the imaging volume, thus reducing ATT sensitivity. Another advantage of flow-sensitized ASL is that placement of a labeling slab is not required, simplifying the planning of the ASL examination, which can be complicated in the kidneys. Thus far, flow-sensitized perfusion measurements have been demonstrated primarily in the brain,[11,13,14,16,17] with recent applications in the heart[18,19] and placenta.[20,21] We recently investigated the feasibility of VSASL labeling in the kidney at 1.5 T, and demonstrated that with properly chosen VSASL sequence parameters, labeling and subtraction artifacts due to (respiratory) motion can be avoided, and with that showed feasibility of VSASL for renal perfusion measurements.[22] Because a low V_C in the presence of respiratory motion can cause spurious labeling of moving tissue, a higher V_C is advised for the kidney than, for example, for the brain ($\approx$ 2 cm/s) with velocity-encoding direction perpendicular to the primary direction of respiratory motion.[11,22] Using VSASL with these appropriate scan parameters for the kidney could, however, shift the label front more upstream in the vascular tree, potentially re-introducing ATT sensitivity. It is therefore essential to characterize the ASL-signal evolution to test how ATT-sensitive VSASL is in the kidney.

In this study, we investigated label dynamics of free-breathing renal VSASL and compared it with the recommended spatially selective pulsed ASL technique FAIR by acquiring ASL data at multiple time points. Moreover, we assessed ATT sensitivity of renal VSASL for different settings of V_C. Finally, we compared RBF values, obtained from a multi-time-point fit, between VSASL and FAIR.

2 | METHODS

This study was approved by the local institutional review board. Written informed consent was obtained from all subjects before the examination.

2.1 | Magnetic resonance imaging

This study was performed on a 1.5T clinical scanner (Ingenia; Philips, Amsterdam, the Netherlands) using a 28-element phased-array receiver coil. All ASL scans were acquired with a single-shot gradient-echo EPI 2D readout in coronal orientation with 80 × 81 acquisition matrix, EPI factor of 55 with feet–head phase encoding, parallel imaging factor 1.5 (SENSE), flip angle of 90º, 3 × 3 × 6 mm acquired voxel size, and a phase-encoding bandwidth of 30.9 Hz/pixel. B_0 shimming was performed for the entire FOV of 244 × 244 mm. A single coronal-oblique slice was acquired along the long axis of the kidneys to minimize through-plane motion due to respiration; single-slice acquisition was chosen for the current study to ensure measurement at a well-defined time point, although multislice readout is an equally feasible

readout option. For FAIR acquisitions, care was taken to exclude the descending aorta from the selective inversion slab (Supporting Information Figure S5). A spectrally selective partial inversion pulse was used for fat suppression, and saturation slabs were placed superior and inferior of the imaging volume to suppress undesired signal aliasing. A recovery delay of 3500 ms was inserted for all VSASL acquisitions, to allow inflow of fresh blood before application of the subsequent labeling pulse (Figure 1).

Background signal was suppressed using two hyperbolic secant inversion pulses performed after labeling. Background suppression (BGS) inversion pulse timings were adapted for each postlabeling delay (PLD), to achieve at most 90% suppression of the kidney signal, based on Bloch simulations performed in *MATLAB* (Release 2019b; The MathWorks, Natick, MA) considering kidney T_1 values from literature of 1057-1183 ms in the cortex and 1389-1573 ms in the medulla.[23] The BGS inversion efficiency was assumed to be 0.95 (ie, loss of 5% of the ASL signal) for each BGS pulse that was applied.

2.2 | Velocity-selective label preparation

In VSASL, blood label is generated by application of motion-sensitizing gradients. In the label condition, the velocity-selective (VS) module includes those motion-sensitizing gradients, which will saturate spins that flow faster than the cutoff velocity V_C, whereas in the control condition, motion-sensitizing gradients are turned off and the blood magnetization remains untouched.[11] In dual VSASL, a second VS module is applied right before image readout, which has equal flow-sensitizing gradients enabled in both the control and label condition, which eliminates signal of blood with $v > V_C$, and thus removes signal from large veins and arteries.[11] Both VS modules will attenuate the VSASL signal due to T_2 relaxation and diffusion weighting, which should be taken into account in the quantification.[11,22]

At the start of the sequence, 4 water excitation technique (WET) saturation pulses[24] were applied to the imaging region (called postsaturation), to eliminate residual magnetization modulation from previous measurements. Postsaturation was followed by a fixed recovery delay of 3.5 seconds, so that each measurement had the same starting magnetization.

2.3 | Flow alternating inversion-recovery label preparation

Flow alternating inversion-recovery labeling was implemented as previously described.[25] Briefly, a slab-selective inversion containing the imaging slice is used in the control condition and a nonselective inversion is used in the label condition. An adiabatic frequency offset–corrected inversion pulse (FOCI) was used for both the selective and nonselective inversion.[26,27] To minimize signal differences caused by inversion-profile differences of the selective and nonselective FOCI pulses, presaturation using WET and postsaturation using a single 90° pulse were applied to the imaging region directly before and after the inversion pulse, respectively. The selective inversion slab was 10 mm wider than the slice thickness.

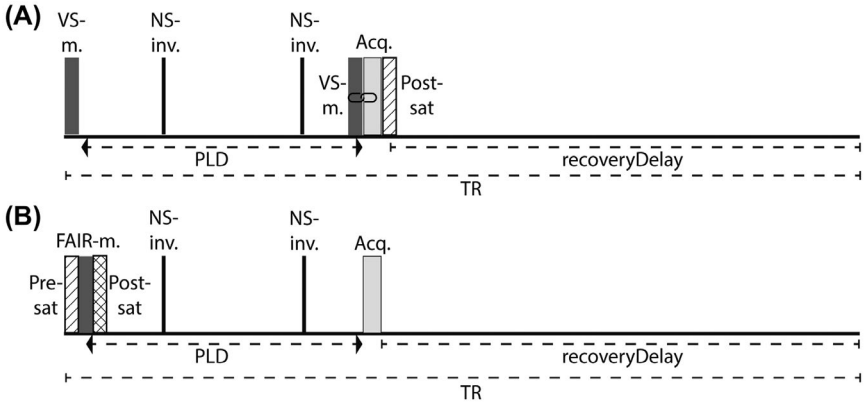

FIGURE 1 A, Velocity-selective arterial spin labeling (VSASL) sequence timings for one repetition time (TR). A velocity-selective (VS) labeling module at the start of the sequence is followed by a postlabeling delay (PLD), during which two nonselective (NS) inversions for background suppression were applied, and right before image acquisition (Acq), a second VS module was applied. Note that the second VS module is linked to the image-acquisition module and shifts with the PLD accordingly. The sequence ends with a postsaturation pulse to eliminate residual magnetization modulation for the following measurements. B, Flow alternating inversion-recovery (FAIR) sequence timings for one TR. A presaturation pulse was applied before, and a postsaturation after, the FAIR labeling module. During the PLD, two nonselective inversions pulses were applied, followed by the image acquisition. Note: Diagram timings are not to scale

2.4 | Magnetic resonance imaging experiments

In addition to the main experiments, we first determined the contribution of diffusion weighting and eddy currents to the VSASL signal in an agarose phantom, especially focusing on acquisitions with short PLD. (See the Supporting Information for detailed methods and results.)

In 7 healthy subjects (age 23-34, 2 men), VSASL and FAIR renal ASL data were acquired during free breathing. Sequence diagrams are illustrated in Figure 1. For both ASL techniques, measurements were performed at five time points (PLD = 400, 800, 1200, 2000, 2600 ms). The VSASL-signal curves were sampled for three different cutoff velocities: 10 cm/s (VSASL10), which has been demonstrated to limit spurious labeling originating from bulk motion of the kidney,[22] and 5 cm/s and 15 cm/s (VSASL5 and VSASL15, respectively). Variation of cutoff velocity was achieved by increasing the gradient strength only, keeping the effective VS-module duration of 50 ms constant. To minimize the risk of spurious labeling, VSASL flow-sensitizing gradients were applied in the anterior–posterior direction.[22] Background-suppression inversion-pulse timings are listed in Table 1.

Data for each PLD were obtained in separate acquisitions that consisted of 13 label–control pairs. The protocol was organized in sets that contained all PLDs for a given ASL technique (or V_C setting) as well as a separately acquired M_0 image. The order of the sets as well as the order of acquisitions at different PLDs within a set was randomly altered between subjects. T_1 mapping was performed once, at the end of the protocol. The M_0 image, essentially the FAIR/VSASL scan with neither labeling nor BGS pulses was acquired with three repetitions that, after realignment, were averaged to improve the SNR. For VSASL, the M_0 image was acquired including the RF pulses of the VS label, but with motion-sensitizing gradients disabled, to achieve similar T_2 weighting as in the ASL-subtraction images. A T_1 map was acquired using a cycled multislice inversion-recovery sequence[28] with 11 inversion times, which was used for kidney region segmentation as well as to provide voxelwise T_1 values for perfusion quantification.

TABLE 1 Sequence timings for both ASL techniques

	PLD (ms)	TR (ms)	BGS timings (ms) inversion 1/inversion 2
VSASL	400	4300	70/305
	800	4700	70/600
	1200	5100	70/830
	2000	5900	70/1380
	2600	6500	70/1800
FAIR	400	4300	70/305
	800	4700	70/580
	1200	5100	70/800
	2000	5900	70/1480
	2600	6500	70/2000

Note: Background suppression timings are reported with respect to the end of the presaturation in FAIR and the end of the first VS module for VSASL acquisitions.

2.5 | Data analysis

Image processing and analyses were performed using custom scripts in *MeVisLab* (version 2.8.2; MeVis Medical Solutions, Bremen, Germany).

Retrospective motion correction was performed using the Elastix toolbox[29] with a B-spline interpolator, an adaptive stochastic gradient descent optimizer and a B-spline stack transform. Cross-contrast registration problems introduced by BGS and parameter differences between sequences were accounted for using a principal component analysis–based group-wise metric.[30] Motion correction was applied separately per kidney. Whole kidney contours were drawn manually on the M_0 image. Before registration, images were cropped to the size of the kidney to reduce processing time.

Voxel-wise T_1 relaxation time was calculated by fitting a mono-exponential recovery function to the intensity of the 11 inversion-recovery images. Per subject, the resulting T_1 map was used for subsequent segmentation of the whole-kidney region of interest into three regions: cortex, medulla, and other (including renal collecting system and veins). Segmentations were done using the Otsu method, an intensity-based thresholding approach[31] with manual threshold adaptation based on the intensity histogram where needed. To avoid partial-volume effects during further analysis, kidney regions were eroded using a 2×2 kernel (Figure 2).

Outlier rejection was applied to registered label-control pairs after subtraction. Subtractions (ΔM) were only included for further analysis when $> 80\%$ (an empirically chosen threshold) voxels within the kidney had a value of less than ± 2 SD from the mean voxel value over all repetitions. With that, additional outliers due to spurious labeling were removed. The remaining subtraction images were averaged over repetitions and divided by the corresponding M_0 for normalization, yielding normalized perfusion-weighted images. Dynamic behavior of the generated label was assessed by calculating the perfusion-weighted signal (PWS = $\Delta M/M_0 \times 100\%$) averaged over cortical voxels in both kidneys for each PLD. Additionally, the measured PWS with VSASL was compensated for T_1 decay by division with $e^{-t/T1}$, using the T_1 of blood with 1350 ms,[32] to facilitate analysis of label accumulation and unraveling of underlying label dynamics. Moreover, the average temporal SNR (tSNR) over all cortical voxels was reported and calculated as the ratio of the mean

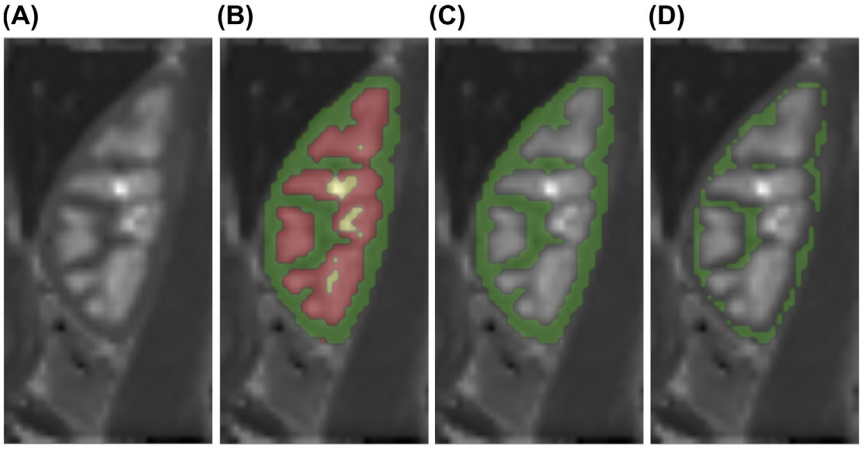

FIGURE 2 A, T_1 map of 1 representative subject. B, Overlay of entire kidney region of interest, segmented into cortex (green), medulla (red), and rest (yellow). C, Overlay of the cortical region, before and (D) after erosion

perfusion-weighted signal over time ($\mu_{\Delta M}$) and the temporal SD ($\sigma_{\Delta M}$): $tSNR = \mu_{\Delta M}/\sigma_{\Delta M}$.

For quantitative analysis, cortical PWS maps were smoothed to reduce noise and stabilize the model fit. A Gaussian kernel with a 1-cm SD was applied specifically to voxels within the cortical mask, using normalized convolution to exclude contributions from voxels outside the mask. Then, voxel-wise RBF (in mL/min/100 g) and ATT (ms) were calculated by fitting Buxton's general kinetic model for pulsed ASL to the multi-PLD data,[4] with modifications for VSASL considering signal contribution from diffusion weighting and the application of a second VS (crusher) module, as previously described (Equation 2).[22]

According to the standard kinetic model, VSASL signal dynamics can be described by three phases:

$$\Delta M_{VSASL} = 0 \quad t < ATT. \tag{1}$$

$$= \alpha_{BGS}^{n} \cdot \beta_{dual} \left(M_0 \cdot \frac{RBF \cdot (t - ATT) \cdot e^{-\frac{t}{T_{1b}}} \cdot q_p(t) \cdot \alpha_{VS}}{6000 \cdot \lambda} + M_{0t} \cdot A_{diffusion} \cdot e^{-\frac{t}{T_{1t}}} \right) \quad ATT < t < ATT + BD. \tag{2}$$

$$= \alpha_{BGS}^{n} \cdot \beta_{dual} \left(M_0 \cdot \frac{RBF \cdot BD \cdot e^{-\frac{t}{T_{1b}}} \cdot q_p(t) \cdot \alpha_{VS}}{6000 \cdot \lambda} + M_{0t} \cdot A_{diffusion} \cdot e^{-\frac{t}{T_{1t}}} \right) \quad t > ATT + BD. \tag{3}$$

For FAIR quantification, the following equations of Buxton's model were used:

$$\Delta M_{FAIR} = 0 \quad t < ATT. \tag{4}$$

$$= \frac{\alpha_{BGS}^{n} \cdot 2M_0 \cdot RBF \cdot (t - ATT) \cdot e^{-\frac{t}{T_{1b}}} \cdot q_p(t) \cdot \alpha_{FAIR}}{6000 \cdot \lambda} \quad ATT < t < ATT + BD. \tag{5}$$

$$= \frac{\alpha_{BGS}^{n} \cdot 2M_0 \cdot RBF \cdot BD \cdot e^{-\frac{t}{T_{1b}}} \cdot q_p(t) \cdot \alpha_{FAIR}}{6000 \cdot \lambda} \quad t > ATT + BD. \tag{6}$$

where α_{BGS} is the BGS inversion efficiency (0.95); β_{dual} is a scaling term to correct for signal attenuation due to the second module application with $e^{(-b \cdot ADC_{kidney})} \cdot \alpha_{VS}$,[22] where b is the b-value of the gradient scheme (varies with V_C); and ADC_{kidney} is the tissue ADC of $2.26 \cdot 10{-}3$ mm^2/s.[33] The value of $A_{diffusion}$ corrects for the expected diffusion attenuation during label condition, and $q_p(t)$ is a dimensionless term as defined in Equation 3 of Buxton et al.[4] The acquired ΔM from multiple PLDs, M_0, and $T_{1tissue}$ values were provided to the corresponding two-compartment model along with assumed values from literature for T_1 of arterial blood at 1.5 T of 1350 ms.[32] The λ is the tissue-blood partition coefficient of 0.9 mL/g,[34] and α_{FAIR} is the labeling efficiency for FAIR (0.95). The M_{0t} is the equilibrium magnetization of tissue. The VS labeling efficiency α_{VS} is determined by T_2 decay during label, $\alpha_{VS} = e^{-TE_{VS}/T_{2b}}$,[11] where TE_{VS} is the duration of a single VS module, and T_{2b} is the T_2 of arterial blood (290 ms at 1.5 T).[35] As we acquired our M_0 images with two VS modules, with RF pulses but without motion-sensitizing gradients, they were attenuated by α_{VS}^2, canceling that factor

in Equations 1-3. In our implementation, PLD was equivalent to *t* in Equations 1-5. This equally applies for VSASL, as we placed the imaging module directly after the second VS module. As is also common in FAIR, the bolus duration (BD) in VSASL therefore refers to the maximum temporal extent of the label bolus that was created in the vasculature.

To stabilize the fitting process, limits for free parameters were provided to the fit. Importantly, these limits were different for the ATT and the RBF determination. To fit the ATT, limits were set to −400 ms to 1000 ms, to allow for negative ATTs that may occur (eg, as a consequence of noise), as anticipated for VSASL. To accommodate those negative ATTs, the upper BD limit provided to the fit was set to 3600 ms, which is larger than our last PLD. However, the VSASL kinetic model[4] in Equations 1-3 provides identical ΔM (PWS) for ATT < 0 as for ATT = 0, and allowing negative ATTs in the RBF fit would result in erroneous RBF values; the reader is referred to Supporting Information Figure S6 for an illustration of Buxton's kinetic model for a different ATT regimen. Hence, for RBF fitting, ATT values were restricted to 0 ms, and the upper BD limit was set to our last measurement point of 2600 ms. Per subject, median values for fit parameters RBF and ATT over all cortical voxels were determined and mean values over all subjects reported. Fitted values for BD are not reported due to the short observation window (0-2600 ms) and less prominent features in the VSASL signal curve.

All statistical analyses were performed using *GraphPad Prism 8* version 8.0.1(244) for Windows (GraphPad Software, San Diego, CA). Differences in fit parameters RBF and ATT between ASL techniques and VSASL V_Cs were tested using paired Friedman or Wilcoxon tests with a significance level of .05 and correction for multiple comparisons.

3 | RESULTS

Phantom experiments verified that contributions of eddy current effects and diffusion attenuation to the VSASL signal were negligible (<0.02% of ΔM). (See the Supporting Information for detailed results.)

Spurious labeling as described in previous literature[22] was observed only with V_C = 5 cm/s in 3 of 7 subjects with one, two, and four affected repetitions, respectively; affected subtraction images were identified and rejected from the analysis by the outlier rejection procedure.

Perfusion-weighted images with clear cortico-medullary contrast were obtained with all ASL techniques for all subjects. This is presented for 1 subject in Figure 3, showing renal perfusion-weighted images acquired during free breathing using VSASL with different cutoff velocities as well as the recommended spatially selective FAIR. The overall PWS of FAIR was higher than the signal measured with VSASL, regardless of the cutoff velocity, which can be explained by labeling by inversion for FAIR versus saturation for VSASL.

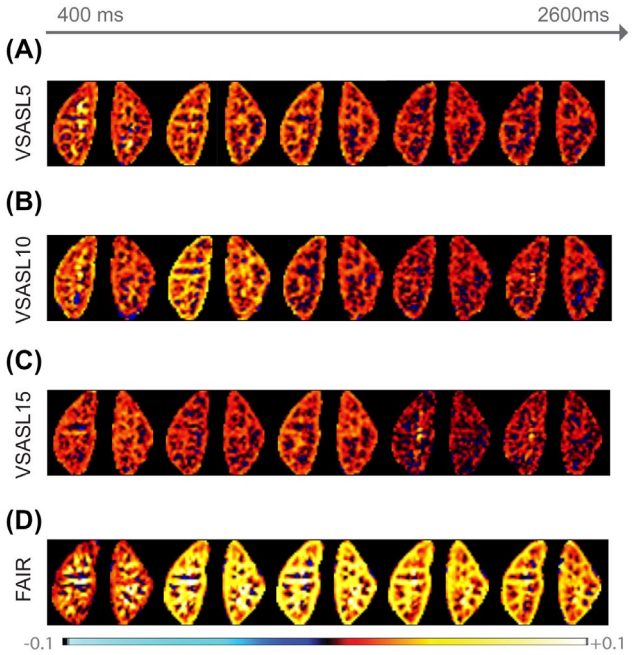

FIGURE 3 Single-slice perfusion-weighted images ($\Delta M/M_0$) of 1 subject acquired at five different time points using FAIR (A), VSASL5 (B), VSASL10 (C), and VSASL15 (D). Scaling was kept constant between techniques to facilitate signal intensity comparison

Figure 4 shows group-average cortical PWS curves for all ASL techniques before (Figure 4A) and after (Figure 4B) T_1 compensation, as well as a linear fit to the first time points (Figure 4C). For subject-level results, the reader is referred to Supporting Information Figure S4. Qualitatively, we observed that at *t* = 400 ms, VSASL curves start much closer to their peak signal (VSASL5 = 63% and VSASL10 = 84%) than FAIR (34%). The PWS curve of VSASL15 was lower than the curves with lower V_Cs, at all time points. The maximum peak PWS generated by flow-based saturation was observed for VSASL10 at approximately 800 ms with a PWS of 3.35 ± 0.83%. For FAIR, using selective inversion, the peak PWS was observed later, at approximately 1200 ms, with 5.98 ± 0.70%.

The same trend was observed regarding the tSNR. Maximum tSNR generated by flow-based saturation was found for VSASL10 with 1.37 ± 0.33, followed by VSASL5 with 1.26 ± 0.26 and VSASL15 with 0.82 ± 0.29. The FAIR method yielded the overall highest tSNR of 3.30 ± 0.72 with selective inversion.

After T_1 compensation, the FAIR PWS curve strongly increased linearly for the whole range of measured time points (Figure 4B). The VSASL PWS curves increased until their peak signal is reached at 800 ms or 1200 ms; after the peak they flattened. This shape suggests a shorter BD and/or shorter ATT for VSASL than for FAIR, as signal accumulation was observed to stop for VSASL at longer PLDs.

In addition, all VSASL signal curves appeared to have their zero crossing near the origin (Figure 4B,C), or in the negative range, indicating label generation inside the tissue, whereas for FAIR the zero crossing is at a later point in the positive range, indicating label generation further away from the target tissue.

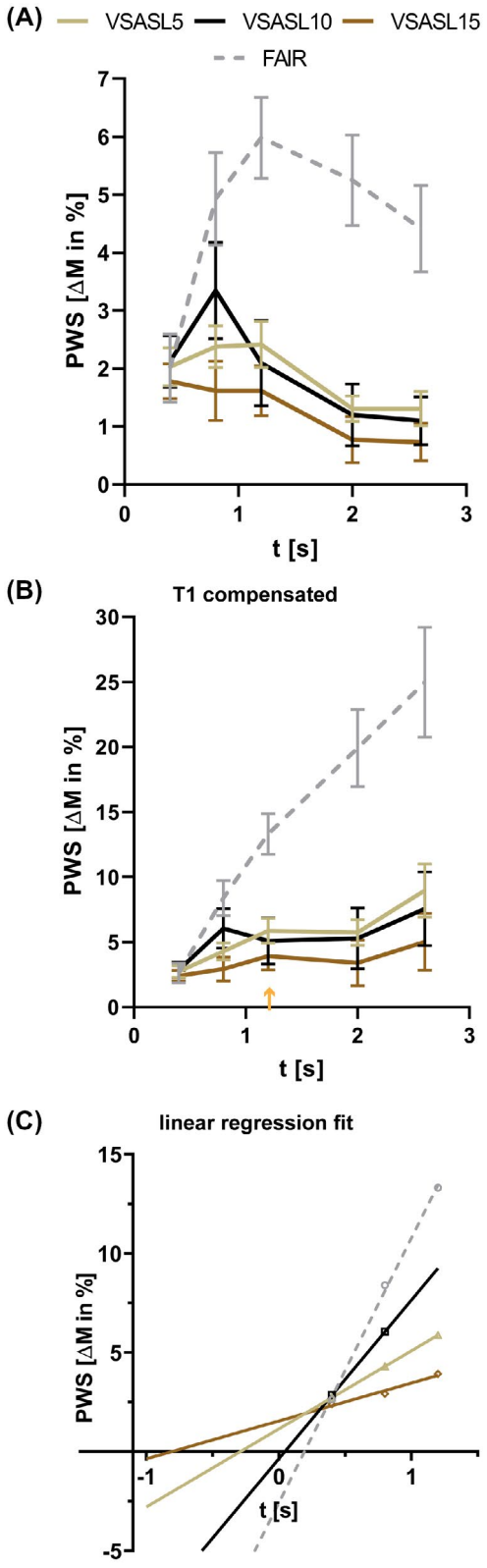

FIGURE 4 A, Group-average arterial spin labeling (ASL) signal curves based on cortical voxels acquired for VSASL5 (gold), VSASL10 (black), and VSASL15 (brown) and FAIR (dashed, gray). B, After T_1 compensation, a peak for VSASL15 is visible at approximately 1200 ms (orange arrow), indicating signal accumulation. C, Linear regression fit on upslope T_1-compensated perfusion-weighted signal (PWS) values per ASL technique. The VSASL curves cross the x-axis on the negative time axis, whereas FAIR crosses zero at positive time *t*

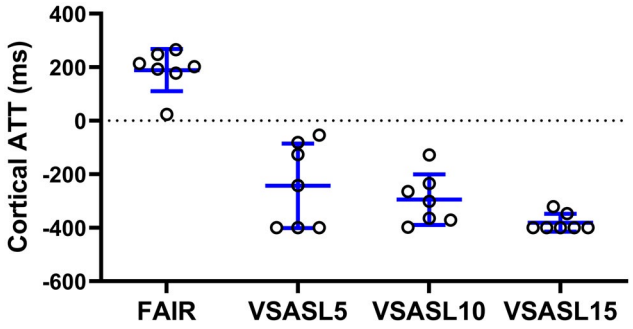

FIGURE 5 Average quantified cortical arterial transit time (ATT) on individual level ($N = 7$) for FAIR and VSASL with cutoff velocities of 5 cm/s, 10 cm/s, and 15 cm/s (VSASL5, VSASL10 and VSASL15), resulting from multiple PLD fits. The VSASL group-average ATTs are negative, whereas FAIR has a positive ATT. Blue lines indicate the mean and SD

Quantitative results from the fitting of multi-PLD ASL data for FAIR and VSASL to Equations 1-5 show group-average cortical ATT for VSASL smaller than 0 ms, independent of the V_C (Figure 5 and Table 2) ($P > .05$). The absence of positive ATTs for VSASL indicates label generation close to or inside the target tissue, and with that supports the hypothesized property of ATT insensitivity. In contrast, for FAIR, a positive group-average cortical ATT of 189 ± 79 ms was found that is larger than for VSASL for all V_Cs (Figure 5) ($P < .05$). Those quantitative ATT results are in line with our previous qualitative observations based on PWS curves.

Due to low tSNR at late PLDs and the short observation window (0-2600 ms), quantitative BD values did not result in a reliable measure to confirm the qualitative observation of shorter BD for VSASL than for FAIR.

Group-average cortical RBF values of 441 ± 84 mL/min/100 g for FAIR, 398 ± 84 mL/min/100 g for VSASL5, and 472 ± 160 mL/min/100 g for VSASL10 (Figure 6A and Table 2) were found, without a significant difference ($P > .05$). For VSASL15, lower group-average cortical RBF value of 308 ± 84 mL/min/100 g was found ($P < .05$). The RBF correlation analysis (Figure 6B) between FAIR and VSASL with different V_Cs showed good correlation on an individual level, as supported by linear regression R^2 values of 0.71 for VSASL5, 0.80 for VSASL10, and 0.61 for VSASL15 (all with respect to FAIR).

	RBF (mL/min/100 g)	Significantly different from	ATT (ms)	Significantly different from
VSASL5	398 (84)	VSASL15	−243 (158)	FAIR
VSASL10	472 (160)	VSASL15	−295 (94)	FAIR
VSASL15	308 (84)	FAIR, VSASL5, VSASL10	−381 (33)	FAIR
FAIR	441 (84)	VSASL15	+189 (79)	VSASL5, VSASL10, VSASL15

TABLE 2 Summary of quantification results

Note: Group-average cortical RBF and ATT after ASL quantification, with SD in brackets, for VSASL with cutoff velocities of 5, 10, and 15 cm/s (VSASL5, VSASL10 and VSASL15) as well as FAIR. Significant differences ($P < .05$) are listed in separate columns (gray) for RBF and ATT.

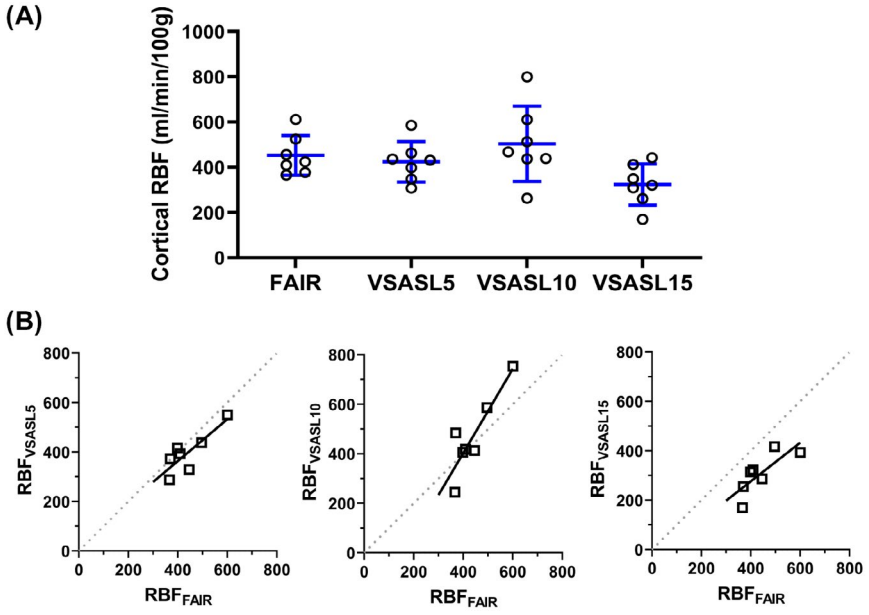

FIGURE 6 A, Average quantified cortical renal blood flow (RBF) on individual level ($N = 7$) for FAIR and VSASL with cutoff velocities of 5 cm/s, 10 cm/s, and 15 cm/s (VSASL5, VSASL10, and VSASL15), resulting from multiple PLD fits. Blue bars indicate the mean and SD. B, Correlation plots with linear regression lines (black) of cortical RBF values measured with FAIR and VSASL cutoff velocities of 5 cm/s, 10 cm/s, and 15 cm/s. Lines of identity are presented in dotted gray lines

4 | DISCUSSION

In this study, we investigated the label dynamics of quantitative VSASL in the kidney and compared those with spatially selective FAIR ASL at 1.5 T. We found that ASL label dynamics in the kidney differed between spatially selective FAIR and flow-sensitive VSASL (Figure 3). The VSASL technique generated relatively high signal already at the shortest PLD, which indicates label generation closer to tissue, and correspondingly a shorter ATT was found for VSASL than for FAIR, for all cutoff velocities studied (Figure 4A). Additionally, quantified VSASL ATT was ≤ 0 ms for all cutoff velocities, supporting ATT insensitivity also for the higher cutoff velocities (>10 cm/s) that have previously been demonstrated to avoid (respiratory) motion corruption of the VS labeling in the kidney during free-breathing acquisitions. After T_1 compensation, perfusion signal increase building toward a peak at 800-1200 ms was observed for VSASL for all cutoff velocities (Figure 4B), supporting that we were indeed measuring label accumulation. Results showed that absolute signal strength as well as tSNR varied as a function of cutoff velocity, and peak PWS and tSNR were maximum for VSASL10 (Figure 3). The T_1-compensated curves suggest a shorter BD for VSASL than for FAIR; however, this remains to be confirmed quantitatively. Finally, quantitative RBF values of VSASL with cutoff velocities of 5 cm/s and 10 cm/s showed good correlation with RBF measured using FAIR.

In the kidney, previous studies of FAIR label dynamics reported a mean ATT in the range of 110 ms to 500 ms[36,37] as well as a peak signal at about 1400 ms,[37] which is similar to the observations from this study with an ATT of about 200 ms and a peak at about 1200 ms. For comparison, the mean ATT values reported for pseudo-continuous ASL, with labeling above the kidneys, range from 700 ms to 1230 ms.[36,37] So far, experience with VSASL and its label dynamics in the kidneys is limited. In the brain, however, a VSASL study with lower cutoff velocities around 2 cm/s also showed insensitivity of average VSASL signal in gray matter to arterial transit delay effects, with high signal already at early time points, quickly followed by the peak signal and rapid

signal decay right after the peak.[13] Moreover, that study also showed pulsed ASL label dynamics with larger transit delay and a later peak, as compared with VSASL; hence, our findings in the kidney are largely in line with these findings in the brain.

The value of V_C affected the label dynamics qualitatively and quantitatively. First, for $V_C = 15$ cm/s, the PWS signal was lower at all time points than for the other V_Cs studied, which was also reflected in an RBF value that was low compared with $V_C = 5$ cm/s and 10 cm/s, and FAIR. We hypothesize that this reflects the limited blood volume flowing with velocities exceeding 15 cm/s in the anterior–posterior direction, at least during part of the cardiac cycle. In brain VSASL literature, those signal magnitude differences have already been attributed to variations in the blood pool, which is labeled as a function of V_C.[38] Similarly, in the myocardium, a reduction of ASL signal with higher V_C (10-40 cm/s) has been observed.[18]

Interestingly, at 800 ms we observed consistently higher signal for VSASL10 than for VSASL5. The exact cause of this observation remains unclear, but might be related to the orientation of vasculature with respect to the flow-encoding gradient (especially near the front end of the label bolus) and/or a mismatch of the effect of velocity-selective saturation for the blood flow velocity distributions during the labeling (first VS module) and crushing condition (second VS module).

We obtained relatively high cortical RBF values (441 ± 84 mL/min/100 g for FAIR and 472 ± 160 mL/min/100 g for dual VSASL10) as compared with previously reported mean cortical RBF values ranging from 195 to 362 mL/min/100 g measured using FAIR,[37,39-41] 158-410 mL/min/100 g using pseudo-continuous ASL,[2,37] and 264 ± 34 mL/min/100 g using dual VSASL.[22] However, several factors may have played a role here: differences in VSASL sequence settings such as velocity-encoding direction and cutoff velocity, BGS application, outlier detection, motion correction, as well as choices of kinetic model fit parameter initialization and limits. An important factor is the definition of the cortical region of interest, which in our study was performed rather strictly to provide cortical values relatively unaffected by partial volume with medulla or background.

Furthermore, for all VSASL experiments, the mean ATT tended to be negative. Negative ATTs have also been reported in a previous study fitting multi-PLD VSASL data in the brain,[13] which attributed those negative values to noise. We support the hypothesis that noise contributes to negative ATTs—especially because we observed that with the reduced PWS for VSASL15 (ie, lowest tSNR), ATT was more negative. The absence of positive ATTs for VSASL supports its ATT insensitivity, which was also observed for higher V_Cs, thereby justifying use of higher V_Cs for renal perfusion measurements, free from motion-induced spurious labeling.

Fitted BD values were not reported in this work, as we experienced that the low tSNR and the range of acquired PLDs limit their accuracy. This should not affect quantification of RBF as long as PLD < BD, and we assume ATT = 0 in the fit. The BD is anchored in the later parts of the curve, around and much after the peak, which are most affected by low tSNR due to T_1 decay. Although, based on our qualitative results, VSASL BD appears to be shorter than FAIR BD (Figure 4A) as a more rapid signal decay of VSASL curves after the peak (as compared with FAIR) was found. Even after T_1 compensation in Figure 4B, VSASL curves do not follow a linear increase, as compared with FAIR.

The lower tSNR for VSASL than for FAIR (saturation vs inversion)[11,13,16] may affect fit stability and with that introduce a larger dependency on limits for the free fit parameters, ATT and BD. Considering that we consistently measured a peak PWS at 800 ms for VSASL10 (Supporting Information Figure S4) and our results indicated ATT insensitivity (ATT = 0), for robust VSASL RBF quantification, it might be more profitable to acquire single-time-point VSASL, without the need of fitting the parameters ATT and BD. Note that this single time point should not be chosen too late, as information on the RBF is mostly in the increase of the (T_1-compensated) PWS up to 800-1000 ms, before the end of the bolus and substantial T_1 decay of the signal occurs. At the same time, single-time-point measurements would be more time efficient and allow us to acquire a higher number of repetitions to increase SNR.

To increase the SNR of velocity-selective labeling, promising methods have been presented, such as velocity-selective inversion[14] and repeated application of velocity-selective saturation modules.[13] First attempts of their application in the kidney have recently been performed in the kidney and yielded promising results.[42]

Conversely, we cannot expect ATT-insensitive VSASL to be very useful in applications in which the ATT differences are important; here, alternative ATT-sensitive, spatially selective ASL methods should be considered. This was already demonstrated in the brain in a study including Moyamoya patients,[17] in which VSASL was used to accurately measure cerebral blood flow, and a spatially selective–pulse ASL technique was used to measure the ATT. In cases of transit delays in the brain, like in patients with Moyamoya and carotid occlusion, perfusion could be underestimated when acquiring single-time-point spatially selective ASL.[17,43] Instead, multi-time-point methods were suggested when spatially selective ASL is applied in those patient groups.[43] However, VSASL was also presented as a more accurate single-time-point alternative.[17] Multi-time-point measurements may not be clinically desirable, as they lengthen scan time. Hence, the strength of ATT-insensitive VSASL lies in the scenario of pathological conditions with slower blood flow, such as renal artery stenosis,[44] or

occlusion of segmental arteries, providing accurate perfusion measurement with quick single-time-point measurement. In such patient populations with high probability of ATT delays, this advantage could be nicely demonstrated. Nevertheless, clinical applicability of VSASL in renal patients should still be investigated.

5 | CONCLUSIONS

The results of this study show that the flow-based VSASL labeling method reduced ATT sensitivity for free-breathing renal perfusion measurement, as compared with FAIR. The ATT sensitivity was still reduced for $V_C = 10$ cm/s, which allows for free-breathing renal perfusion measurements free from motion-induced spurious labeling. Hence, this method has potential as an ATT-insensitive technique for time-efficient RBF measurements, despite a lower tSNR than FAIR, in patients in which compromised flow may introduce errors otherwise.

ACKNOWLEDGMENT

The authors thank MeVis Medical Solutions (Bremen, Germany) for providing the medical image processing and visualization environment, which was used for image analysis.

CONFLICT OF INTEREST

Marijn van Stralen is co-founder and shareholder of MRIguidance B.V.

ORCID

Isabell K. Bones https://orcid.org/0000-0002-7916-5013
Suzanne L. Franklin https://orcid.org/0000-0001-6886-5578
Anita A. Harteveld https://orcid.org/0000-0002-3379-0710
Matthias J. P. van Osch https://orcid.org/0000-0001-7034-8959
Sophie Schmid https://orcid.org/0000-0003-0750-7798

REFERENCES

1. Selby NM, Blankestijn PJ, Boor P, et al. Magnetic resonance imaging biomarkers for chronic kidney disease: a position paper from the European cooperation in science and technology action PARENCHIMA. *Nephrol Dial Transplant*. 2018;33(Suppl 2):ii4-ii14.
2. Odudu A, Nery F, Harteveld AA, et al. Arterial spin labelling MRI to measure renal perfusion: a systematic review and statement paper. *Nephrol Dial Transplant*. 2018;33(Suppl 2):ii15-ii21.
3. Nery F, Buchanan CE, Harteveld AA, et al. Consensus-based technical recommendations for clinical translation of renal ASL MRI. *Magn Reson Mater Physics, Biol Med*. 2020;33:141-161.
4. Buxton RB, Frank LR, Wong EC, Siewert B, Warach S, Edelman RR. A general kinetic model for quantitative perfusion imaging with arterial spin labeling. *Magn Reson Med*. 1998;40:383-396.
5. Campbell AM, Beaulieu C. Pulsed arterial spin labeling parameter optimization for an elderly population. *J Magn Reson Imaging*. 2006;23:398-403.
6. Liu Y, Zhu X, Feinberg D, et al. Arterial spin labeling MRI study of age and gender effects on brain perfusion hemodynamics. *Magn Reson Med*. 2012;68:912-922.
7. Richter CS, Krestin GP, Eichenberger AC, Schöpke W, Fuchs WA. Assessment of renal artery stenosis by phase-contrast magnetic resonance angiography. *Eur Radiol*. 1993;3:493-498.
8. Wong EC. An introduction to ASL labeling techniques. *J Magn Reson Imaging*. 2014;40:1-10.
9. Kim S-G. Quantification of relative cerebral blood flow change by flow-sesitive alternating inversion recovery (FAIR) technique: application to functional mapping. *Magn Reson Med*. 1995;34:293-301.
10. Norris DG, Schwarzbauer C. Velocity selective radiofrequency pulse trains. *J Magn Reson*. 1999;137:231-236.
11. Wong EC, Cronin M, Wu WC, Inglis B, Frank LR, Liu TT. Velocity-selective arterial spin labeling. *Magn Reson Med*. 2006;55:1334-1341.
12. Schmid S, Ghariq E, Teeuwisse WM, Webb A, Van Osch MJP. Acceleration-selective arterial spin labeling. *Magn Reson Med*. 2014;71:191-199.
13. Guo J, Wong EC. Increased SNR efficiency in velocity selective arterial spin labeling using multiple velocity selective saturation modules (mm-VSASL). *Magn Reson Med*. 2015;74:694-705.
14. Qin Q, van Zijl PCM. Velocity-selective-inversion prepared arterial spin labeling. *Magn Reson Med*. 2016;76:1136-1148.
15. Duhamel G, De Bazelaire C, Alsop DC. Evaluation of systematic quantification errors in velocity-selective arterial spin labeling of the brain. *Magn Reson Med*. 2003;50:145-153.
16. Schmid S, Heijtel DFR, Mutsaerts HJMM, et al. Comparison of velocity- and acceleration-selective arterial spin labeling with [15O] H2O positron emission tomography. *J Cereb Blood Flow Metab*. 2015;35:1296-1303.
17. Bolar DS, Gagoski B, Orbach DB, et al. Comparison of CBF measured with combined velocity-selective arterial spin-labeling and pulsed arterial spin-labeling to blood flow patterns assessed by conventional angiography in pediatric Moyamoya. *Am J Neuroradiol*. 2019;40:1842-1849.
18. Jao TR, Nayak KS. Demonstration of velocity selective myocardial arterial spin labeling perfusion imaging in humans. *Magn Reson Med*. 2017;272-278.
19. Landes V, Javed A, Jao T, Qin Q, Nayak K. Improved velocity-selective labeling pulses for myocardial ASL. *Magn Reson Med*. 2020;84:1909-1918.
20. Zun Z, Limperopoulos C. Placental perfusion imaging using velocity-selective arterial spin labeling. *Magn Reson Med*. 2018;80:1036-1047.
21. Harteveld AA, Hutter J, Franklin SL, et al. Systematic evaluation of velocity-selective arterial spin labeling settings for placental perfusion measurement. *Magn Reson Med*. 2020;84:1828-1843.
22. Bones IK, Franklin SL, Harteveld AA, et al. Influence of labeling parameters and respiratory motion on velocity-selective arterial spin labeling for renal perfusion imaging. *Magn Reson Med*. 2020;84:1919-1932.

23. Huang Y, Sadowski EA, Artz NS, et al. Measurement and comparison of T1 relaxation times in native and transplanted kidney cortex and medulla. *J Magn Reson Imaging*. 2011;33:1241-1247.
24. Ogg RJ, Kingsley PB, Taylor JS. WET, a T1- and B1-insensitive water-suppression method for in vivo localized 1H NMR spectroscopy. *J Magn Reson Ser B*. 1994;104:1-10.
25. Martirosian P, Klose U, Mader I, Schick F. FAIR true-FISP perfusion imaging of the kidneys. *Magn Reson Med*. 2004;51:353-361.
26. Ordidge RJ, Wylezinska M, Hugg JW, Butterworth E, Franconi F. Frequency offset corrected inversion (FOCI) pulses for use in localized spectroscopy. *Magn Reson Med*. 1996;36:562-566.
27. Yongbi MN, Branch CA, Helpern JA. Perfusion imaging using FOCI RF pulses. *Magn Reson Med*. 1998;40:938-943.
28. Clare S, Jezzard P. Rapid T1 mapping using multislice echo planar imaging. *Magn Reson Med*. 2001;45:630-634.
29. Klein S, Staring M, Murphy K, Viergever MA, Pluim J. Elastix: a toolbox for intensity-based medical image registration. *IEEE Trans Med Imaging*. 2010;29:196-205.
30. Huizinga W, Poot D, Guyader J-M, et al. PCA-based groupwise image registration for quantitative MRI. *Med Image Anal*. 2016;29:65-78.
31. Hima Bindu C, Satya PK. An efficient medical image segmentation using conventional OTSU method. *Int J Adv Sci Technol*. 2012;38:67-74.
32. Alsop DC, Detre JA, Golay X, et al. Recommended implementation of arterial spin-labeled perfusion MRI for clinical applications: a consensus of the ISMRM Perfusion Study Group and the European Consortium for ASL in Dementia. *Magn Reson Med*. 2015;73:102-116.
33. Sulkowska K, Palczewski P, Duda-Zysk A, et al. Diffusion-weighted MRI of kidneys in healthy volunteers and living kidney donors. *Clin Radiol*. 2015;70:1122-1127.
34. Herscovitch P, Raichle ME. What is the correct value for the brain-blood partition coefficient for water? *J Cereb Blood Flow Metab*. 1985;5:65-69.
35. Stanisz GJ, Odrobina EE, Pun J, et al. T1, T2 relaxation and magnetization transfer in tissue at 3T. *Magn Reson Med*. 2005;54:507-512.
36. Nery F, Gordon I, Thomas D. Non-invasive renal perfusion imaging using arterial spin labeling MRI: challenges and opportunities. *Diagnostics*. 2018;8:2.
37. Harteveld AA, de Boer A, Franklin SL, Leiner T, van Stralen M, Bos C. Comparison of multi-delay FAIR and pCASL labeling approaches for renal perfusion quantification at 3T MRI. *Magn Reson Mater Physics Biol Med*. 2020;33:81-94.
38. Wu WC, Wong EC. Feasibility of velocity selective arterial spin labeling in functional MRI. *J Cereb Blood Flow Metab*. 2007;27:831-838.
39. Gardener AG, Francis ST. Multislice perfusion of the kidneys using parallel imaging: image acquisition and analysis strategies. *Magn Reson Med*. 2010;63:1627-1636.
40. Hammon M, Janka R, Siegl C, et al. Reproducibility of kidney perfusion measurements with arterial spin labeling at 1.5 Tesla MRI combined with semiautomatic segmentation for differential cortical and medullary assessment. *Med (United States)*. 2016;95:1-9.
41. Cutajar M, Thomas DL, Hales PW, Banks T, Clark CA, Gordon I. Comparison of ASL and DCE MRI for the non-invasive measurement of renal blood flow: quantification and reproducibility. *Eur Radiol*. 2014;24:1300-1308.
42. Franklin SL, Bones IK, Harteveld AA, et al. Multi-organ comparison of flow-based arterial spin labeling techniques: spatially non-selective labeling for cerebral and renal perfusion imaging. *Magn Reson Med*. 2021;85:2580-2594.
43. Akiyama T, Morioka T, Shimogawa T, et al. Arterial spin-labeling magnetic resonance perfusion imaging with dual postlabeling delay in internal carotid artery steno-occlusion: validation with digital subtraction angiography. *J Stroke Cerebrovasc Dis*. 2016;25:2099-2108.
44. Lee VS, Rofsky NM, Ton AT, Krinsky GA, Weinreb JC. Contrast MR imaging to measure renal artery velocity waveforms renovascular hypertension. *Am J Roentgenol*. 2000;174:499-508.

SUPPORTING INFORMATION

Additional supporting information may be found online in the Supporting Information section.

FIGURE S1 Raw arterial spin labeling (ASL) control phantom images acquired at multiple time points for cutoff velocities (V_Cs) of 5, 10, and 15 cm/s. Intensity scaling was kept constant for all images

FIGURE S2 A, M_0 equilibrium image of the spherical agarose phantom with a red circle indicating the region of interest (ROI) for perfusion-weighted signal (PWS) analysis. B, Region of interest (ROI) cropped normalized perfusion-weighted images of the velocity-selective ASL (VSASL) scans performed with three different cutoff velocities (5, 10, and 15 cm/s) and five post labeling delays (PLDs) (100, 400, 800, 1200, and 2000 ms). Images have equal look-up table scaling

FIGURE S3 Region-of-interest analysis of background ASL signal obtained from VSASL images acquired in the phantom experiment. Data points represent the mean PWS, calculated over all voxels inside the ROI (shown in Supporting Information Figure S2)

FIGURE S4 Individual ASL signal curves compensated for T_1 decay of the label obtained from cortical voxels acquired for VSASL5 (gold), VSASL10 (black), and VSASL15 (brown) and FAIR (gray)

FIGURE S5 Planning of the flow alternating inversion recovery (FAIR) acquisition. The imaging slab (green) as well as the selective inversion (blue) are covering both kidneys, even in the case of respiratory motion. The primary displacement of the kidney with respiration is in the feet–head direction and angulated along the muscle (psoas major), as indicated by the yellow arrow. Care was taken to exclude the descending aorta (orange) from the selective inversion slab

FIGURE S6 Simplified visualization of the arterial vasculature side, inside and outside of the tissue. A-C, Label scenarios with different arterial transit time (ATT) (delays). The venous vascular side is neglected for readability. The PLD and V_C are the same for all scenarios: For our VSASL experiment, the apparent bolus duration ($BD_{apparent}$) is determined by the PLD. The extension of the generated label (green block, VS-m1) is defined by the cutoff velocity ($V \geq V_C$) and coil coverage. Consequently, the three ATT scenarios (A, B,

and C) result from different velocity distributions inside the tissue

TABLE S1 Sequence timings for both ASL techniques, VSASL and FAIR, including the PLD (column 1), the TR (column 2), and timings of the background-suppression inversion-pulse centers (column 3, defined from the end of the first velocity-selective labeling module)

How to cite this article: Bones IK, Franklin SL, Harteveld AA, et al. Exploring label dynamics of velocity-selective arterial spin labeling in the kidney. *Magn Reson Med*. 2021;86:131–142. https://doi.org/10.1002/mrm.28683